J. Opt. A: Pure Appl. Opt. **11** (2009) 015507 (9pp) doi:10.1088/1464-4258/11/1/015507

Poincaré sphere analysis of a ferroelectric liquid crystal optical modulator: application to optimize the contrast ratio

M M Sánchez-López[1], P García-Martínez[2], A Martínez-García[3] and I Moreno[3,4]

[1] Instituto de Bioingeniería and Departamento de Física y Arquitectura de Computadores, Universidad Miguel Hernández de Elche, 03202 Elche, Spain
[2] Departamento de Óptica, Universitat de València, 46100 Burjassot, Spain
[3] Departamento de Ciencia de Materiales, Óptica y Tecnología Electrónica, Universidad Miguel Hernández de Elche, 03202 Elche, Spain

E-mail: i.moreno@umh.es

Received 21 October 2008, accepted for publication 18 November 2008
Published 18 December 2008
Online at stacks.iop.org/JOptA/11/015507

Abstract
The Poincaré sphere representation is used to analyze the polarization transformation achieved with a ferroelectric liquid crystal (FLC) optical modulator. This device acts as a switchable wave-plate, in which the orientation of the principal axes rotates under the action of an applied bipolar voltage. In the standard operational mode for intensity switching, the rotation angle of the principal axes is $\Delta\theta = \pi/4$ and the phase shift is $\phi = \pi$ (half-wave-plate). However, for wavelengths different from the design one, the FLC deviates from the half-wave-plate performance and the optical contrast is diminished. We use the Poincaré sphere representation to perform a theoretical analysis of the intensity switch performance of the FLC modulator as a function of the phase shift ϕ. Using spherical trigonometric relations we derive analytical expressions for the intensity contrast as a function of ϕ and we show how to compensate its decrease when $\phi \neq \pi$ by using appropriate elliptically polarized illumination. These situations are experimentally demonstrated using a commercially available FLC cell.

Keywords: ferroelectric liquid crystal, Poincaré sphere, birefringence, polarization

(Some figures in this article are in colour only in the electronic version)

1. Introduction

Liquid crystal devices (LCDs) have become attractive for practical applications such as diffractive optics, adaptive optics, or optical metrology [1–3]. LCDs based on ferroelectric liquid crystals (FLCs) are of particular interest because of their very fast frame rates (several kilohertz) and highly efficient electro-optic effect [4–6]. Single-pixel FLC modulators have found applications such as optical switches [7], tunable filters [8], optical rotators [9], and phase shifters [10]. Pixelated FLC displays have also found applications in diffractive optics for the generation of digital holograms [11] or optical tweezers [12].

The SmC* liquid crystal phase used in commercial FLC modulators is biaxial, and the orientation of the optical axes shows slight wavelength dispersion. However, these effects are so small (the biaxiality presents typical values of the order of 10^{-3} for the refractive index difference, and the dispersion of the optical axes is less than one degree for the visible optical range) [13], that an FLC modulator can be approximated as a uniaxially birefringent wave-plate layer, with two stable optical axis orientations with a relative angle $\Delta\theta$ [14]. The extraordinary axis corresponds to the orientation of the liquid crystal (LC) director and it switches between the two stable orientations by changing the sign of an addressed

[4] Address for correspondence: Departamento de Ciencia de Materiales, Optica y Tecnología de Materiales, Universidad Miguel Hernández de Elche, 03202 Elche, Spain.

voltage. For the standard configuration, the orientation of the LC director rotates with a relative angle $\Delta\theta = \pi/4$ and the FLC modulator acts as a half-wave-plate (it introduces a phase shift $\phi = \pi$ radians) for a specific design wavelength [14]. Then, by placing the FLC modulator in between a pair of polarizers with the proper orientation, either a maximum contrasted binary intensity modulation or a binary π phase-only modulation can be achieved. However, as the wavelength of the optical signal varies, so does the phase shift (ϕ). Consequently, at least one of the two emerging polarization states is no longer linear and a decrease in the contrast is observed. This is a detrimental effect that limits its use in the above-mentioned applications. For that reason, compensation techniques to provide an achromatic optimized response for a wide spectral band have been proposed, on the basis of the material dispersion of external wave-plates [9]. Recently we have addressed a related but different problem, which is the optimization for a single but not the design wavelength, and we presented a simple technique for improving the contrast of the optical signal [15]. We employed a quarter-wave-plate in front of the modulator in order to illuminate the device with appropriate elliptically polarized light rather than with linearly polarized light. This type of optimization has been widely and successfully employed to obtain specific modulation responses in other devices like twisted-nematic liquid crystal cells [16, 17].

In our previous work [15], the orientations of the polarization elements (input and output polarizers, and quarter-wave-plate) were numerically searched in order to achieve the optimal intensity contrast. In the present paper we apply the Poincaré sphere representation of the polarization states involved in the FLC switching to provide a physical explanation and an analytical probe of our previously reported numerical optimization procedure. By using this formalism the optimization process of the FLC switching performance is reduced to a simple geometrical problem. Optimal binary intensity modulation is achieved when the two polarization states emerging from the FLC modulator are linear and orthogonal. We show that these characteristics cannot be achieved when ϕ differs from the ideal value of π radians, but we make use of the Poincaré sphere to find polarization configurations that are very close to this ideal situation. Using spherical trigonometric relations, we provide analytical expressions for the intensity contrast as a function of the phase shift ϕ for both the standard configuration (the device is illuminated with linearly polarized light) and the optimized configuration that uses appropriate elliptically polarized light.

The paper is organized as follows. In section 2 we briefly review some properties of the Poincaré sphere formalism which are useful to analyze the polarization transformations upon the action of the FLC modulator. In section 3, this formalism is applied to improve the FLC optical contrast for arbitrary values of the phase shift ϕ. Theoretical expressions of the intensity contrast as a function of ϕ are derived. Experimental verification is outlined in section 4 with a commercially available device. Finally, section 5 summarizes the main conclusions of the work.

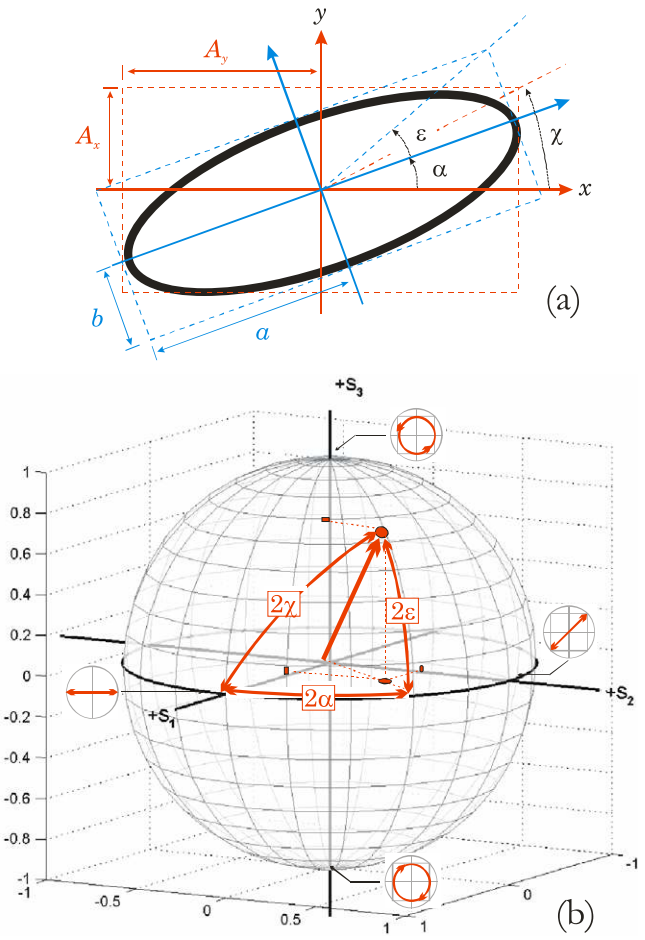

Figure 1. (a) Polarization ellipse and (b) its representation on the Poincaré sphere. ε and α represent the ellipticity and azimuth angles, respectively.

2. Poincaré sphere and the FLC modulator

In this section we review some properties of the Poincaré sphere representation which are useful for our FLC intensity-modulator optimization purpose. This representation has been used in early and modern liquid crystal devices [17–22]. It provides a useful method to represent the polarization states, as well as to visualize their transformation upon the action of different polarization devices. In the Poincaré representation there is a biunivocal correspondence between a polarization state and a point on the sphere surface. Let us consider an arbitrary state described by the Jones vector:

$$J = \begin{pmatrix} A_x \exp(\mathrm{i}\delta_x) \\ A_y \exp(\mathrm{i}\delta_y) \end{pmatrix}. \tag{1}$$

This state of polarization (SOP) can be described typically either in the amplitude's ratio—phase shift (χ, Δ) representation, or in the azimuth—ellipticity (α, ε) representation, as defined in figure 1(a). These angles are derived from equation (1) as [23]

$$\Delta = \delta_y - \delta_x, \tag{2a}$$

$$\tan(\chi) = \frac{A_y}{A_x}, \tag{2b}$$

$$\tan(2\alpha) = \frac{2A_xA_y}{A_x^2 - A_y^2}\cos(\Delta), \tag{2c}$$

$$\tan(\varepsilon) = \frac{b}{a} = \pm\sqrt{\frac{A_x^2\sin^2(\alpha) + A_y^2\cos^2(\alpha) - A_xA_y\cos(\Delta)\sin(\alpha/2)}{A_x^2\cos^2(\alpha) + A_y^2\sin^2(\alpha) + A_xA_y\cos(\Delta)\sin(\alpha/2)}}. \tag{2d}$$

The Stokes vector $\mathbf{S} = (S_1, S_2, S_3)$ is defined in terms of the normalized Stokes parameters, which are calculated from the previous angles as

$$S_1 = \cos(2\chi) = \cos(2\varepsilon)\cos(2\alpha), \tag{3a}$$

$$S_2 = \sin(2\chi)\cos(\Delta) = \cos(2\varepsilon)\sin(2\alpha), \tag{3b}$$

$$S_3 = \sin(2\chi)\sin(\Delta) = \sin(2\varepsilon). \tag{3c}$$

The direct analogy of these equations with the spherical coordinates allows the univocal representation of any SOP on the Poincaré sphere. The three positive orthogonal axes (S_1, S_2 and S_3 in figure 1(b)) denote, respectively, linear polarizations at 0°, 45°, and L circular polarization. The equator circle is the locus of the linearly polarized states, whereas the elliptically polarized states lie on the rest of the sphere surface. The longitude (2α) and latitude (2ε) of a surface point define the azimuth and the ellipticity angles, respectively. These angles can be expressed in terms of the Stokes parameters from equation (3) as

$$\alpha = \frac{1}{2}\arctan\left(\frac{S_2}{S_1}\right), \qquad -\frac{\pi}{2} \leqslant \alpha \leqslant \frac{\pi}{2}, \tag{4a}$$

$$\varepsilon = \frac{1}{2}\arcsin(S_3), \qquad -\frac{\pi}{4} \leqslant \varepsilon \leqslant \frac{\pi}{4}. \tag{4b}$$

Some properties of the Poincaré sphere, especially relevant for our purpose, are the following:

(I) From equation (4*a*) equi-azimuth SOPs are given by a constant value of S_2/S_1. Thus, they lie on a sphere meridian. On the other hand, equi-ellipticity SOPs have a constant value of S_3 (see equation (4*b*)), i.e., they lie on a sphere parallel.

(II) Two polarization states SOP_a and SOP_b are orthogonal if they are located on antipodal points. They share the same ellipticity but opposite helicity (i.e., $\varepsilon_a = -\varepsilon_b$), and their azimuths fulfil $\alpha_b = \alpha_a \pm \pi/2$. The scalar product of their Stokes vectors, $\rho = \mathbf{S}_a \cdot \mathbf{S}_b$, is equal to -1. According to this scalar product the degree of orthogonality (τ_o) between two SOPs can be defined as $\tau_o = (1-\rho)/2$, with $\tau_o = 1$ for two perfectly orthogonal states and $\tau_o = 0$ for two equal states.

(III) The action of a linear retarder (wave-plate), with phase shift ϕ and orientation θ, on the polarization states is visualized as a ϕ-rotation of the sphere along the axis defined by 2θ [23]. This is illustrated in figure 2(a), where F and S denote the wave-plate fast and slow axes. This actuation shows that two SOPs that traverse a wave-plate keep their relative degree of orthogonality (τ_o) at the output, since the angle between the corresponding Stokes vectors is maintained after the sphere rotation.

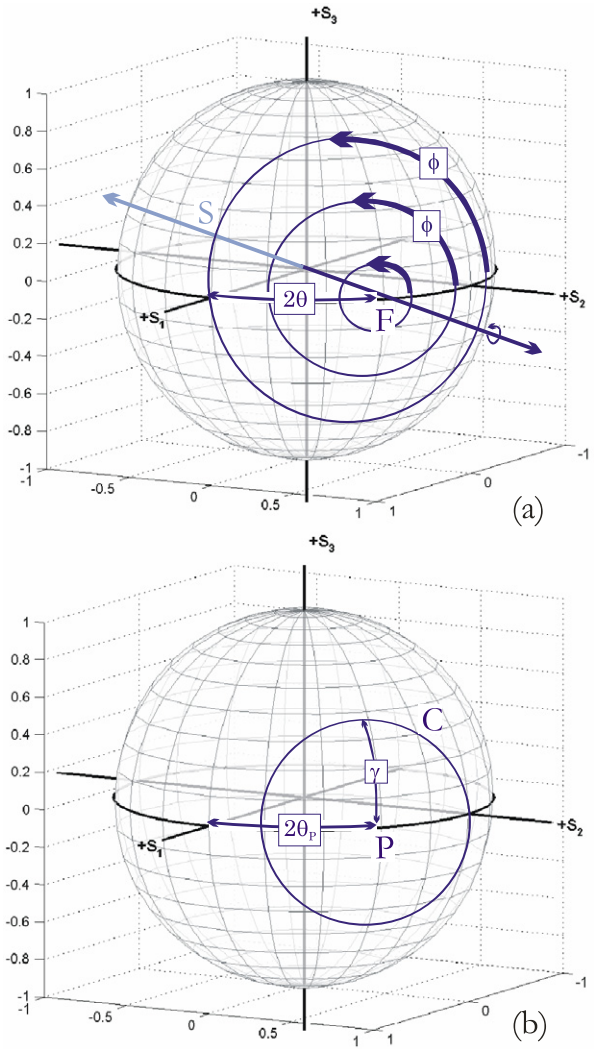

Figure 2. Visualization on the Poincaré sphere of: (a) action of a generic linear wave-plate with orientation θ (points F and S denote the fast and slow axes) and phase shift ϕ. (b) Projection of polarization states onto a linear polarizer with orientation θ_P (point P denotes the linear state that is fully transmitted) and γ is the projection angle. All points on circle C transmit with equal intensity.

(IV) A quarter-wave-plate (QWP) can be used to transform a pair of orthogonal arbitrary SOPs onto a pair of orthogonal linear SOPs. This is obtained by simply orienting the QWP fast axis coincident with the azimuth of one of the elliptical states. Then, the phase shift $\phi = \pi/2$ rotates the antipodal points in such a way that they are translated onto antipodal points located on the equator of the sphere.

(V) Finally, figure 2(b) shows the projection of an arbitrary SOP onto a linear polarizer, with orientation θ_P. All points lying on a circle that keeps an angle γ with the state fully transmitted by the polarizer (point P in figure 2(b)) transmit with equal normalized intensity $i = \cos^2(\gamma/2)$; this is known as the generalized Malus law [24].

Figure 3 shows the FLC modulator performance as a binary intensity modulator in the standard operational mode. The LC director switches between two stable orientations upon addressing an electric field, with an overall LC rotation angle

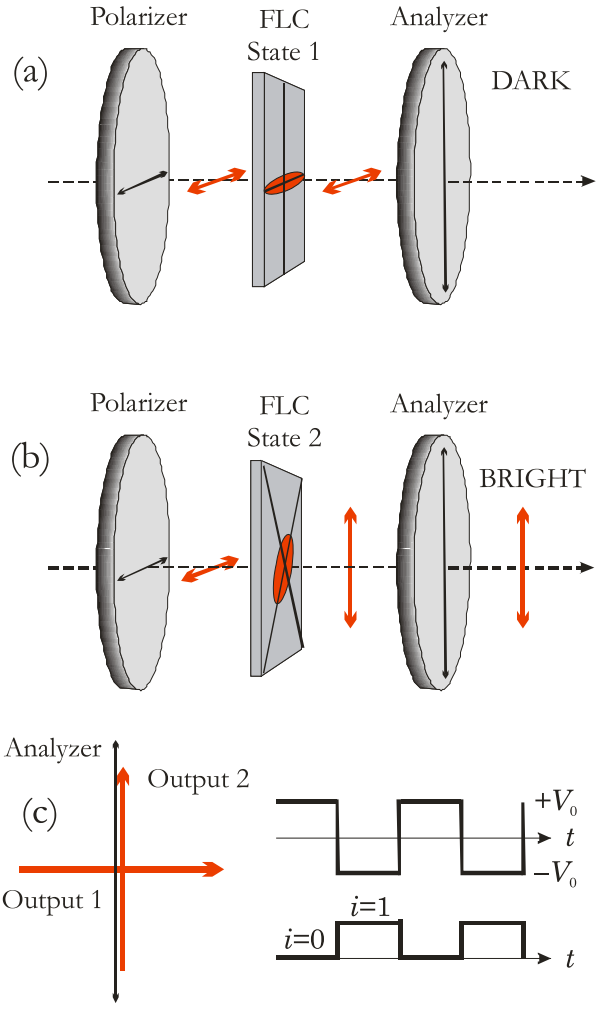

Figure 3. Standard operational mode of the FLC modulator (phase shift $\phi = \pi$ and rotation angle $\theta = \pi/4$). Input polarization is parallel to the LC director at state 1. (a) State 1: output and input polarizations are parallel. (b) State 2: output polarization is rotated by $\pi/2$. (c) Analyzer configuration for binary intensity modulation $i(t)$ as a function of the addressed voltage $V(t)$.

of $\Delta\theta = \pi/4$ and a phase shift of $\phi = \pi$ radians (i.e. the FLC acts as a half-wave-plate). We assume the two stable LC molecular orientations at $\theta = 0$ and $\pi/4$ and the input linearly polarized light with orientation $\alpha = 0$. This state leaves the FLC modulator without change in the first LC position (figure 3(a)). When the FLC director switches to the second stable position, the typical half-wave action yields a $\pi/2$ rotation of the output linear polarization (figure 3(b)). Thus, the device acts as a perfect binary intensity modulator if the analyzer is oriented parallel to one of these two output linear states, since one is fully transmitted while the orthogonal state is fully absorbed. Consequently, this configuration modulates the transmitted intensity with maximum contrast (figure 3(c)).

Since the FLC modulator acts as a switchable wave-plate, its action on an arbitrary SOP is described on the Poincaré sphere by two rotations around two different axes defined by the two LC director orientations, in our case 0 (rotation around the S_1 axis) and $\pi/4$ (rotation around the S_2 axis), respectively. In the ideal situation sketched in figure 3, these two rotations are of $\phi = \pi$ radians and transform any input linear SOP onto a pair of output SOPs which are linear and orthogonal [15]. However, when ϕ differs from the ideal π value the two rotations lead, in general, to elliptical states, and the performance presented in figure 3 is lost.

3. Poincaré sphere transformations for an arbitrary phase shift

In this section we illustrate the Poincaré sphere transformations for arbitrary values of the phase shift ϕ. In all cases we will consider that the rotation angle is fixed: $\Delta\theta = \pi/4$ (it does not depend on the operating wavelength). For representation in figures, we consider the specific phase shift $\phi = 135°$, which corresponds to our device when being illuminated with a He–Ne laser of wavelength $\lambda = 633$ nm [15].

3.1. Contrast reduction in the standard configuration

We start by analyzing the standard modulation scheme described in figure 3. Figure 4(a) shows the transformation induced by the two stable LC positions. Output SOP1 (asterisk marker) coincides with the input state (black circular marker) since the rotation around the S_1 axis does not affect this input SOP (this linear polarization coincides with the principal axis of the FLC modulator in state 1). However, the rotation of the sphere around the S_2 axis leads to an output state 2 in general located outside the equator plane (diamond marker), thus corresponding to an elliptically polarized state. This elliptical state has its major and minor axes centered on the x–y axes regardless of the value of ϕ (the azimuth is $\alpha = 0$ for $\phi \in [0, \pi/2]$ and $\phi \in [3\pi/2, 2\pi]$, or $\alpha = \pi/2$ for $\phi \in [\pi/2, 3\pi/2]$). Only when the phase shift is $\phi = \pi$ radians, does the rotation around the S_2 axis lead to an output state located at the equator plane, which corresponds to an output SOP2 which is linear and orthogonal to output SOP1. The geometry of figure 4(a) shows that the ellipticity (ε_2) of SOP2 is directly related to the phase shift value through the following relations:

$$2\varepsilon_2 = \begin{cases} -\phi & \text{if } \phi \in [0, \frac{\pi}{2}] \\ \phi - \pi & \text{if } \phi \in [\frac{\pi}{2}, \frac{3\pi}{2}] \\ 2\pi - \phi & \text{if } \phi \in [\frac{3\pi}{2}, 2\pi]. \end{cases} \quad (5)$$

If the analyzer is kept in the vertical orientation (figure 3), these two output SOPs are projected onto the point located at coordinates ($S_1 = -1, S_2 = 0, S_3 = 0$) (point P in figure 4(a)). Following the generalized Malus law sketched in figure 2(b), the intensity for the first state is always $i_1 = 0$, and the contrast $c = |i_2 - i_1|$ is reduced to the value

$$c = i_2 = \cos^2(\varepsilon_2) = \sin^2\left(\frac{\phi}{2}\right). \quad (6)$$

This is the analytical expression for the intensity contrast as a function of ϕ in the standard operational mode. In table 1 (left columns) we give the polarization parameters for the configuration shown in figure 4(a) and for the specific value $\phi = 135°$ of our device. The degree of orthogonality between the two output SOPs is $\tau_o = 0.853$ and the intensity contrast is reduced to $c = 0.853$.

Table 1. Polarization parameter values for different configurations for an FLC modulator with phase shift $\phi = 135°$. The standard configuration has the input polarizer oriented at 0°. The optimized configuration has the input polarizer oriented at 22.5° and a QWP behind the FLC modulator oriented at −22.5°.

	Standard configuration (figure 4(a)) $S_{\text{input}} = (1, 0, 0)$		Optimized polarization (figure 4(b)) $S_{\text{input}} = (0.707, 0.707, 0)$			
			SOPs behind FLC		SOPs behind QWP	
	Output1	Output2	Output1	Output2	Output1′	Output2′
S_1	1	−0.707	+0.707	−0.500	+0.250	−0.250
S_2	0	0	−0.500	+0.707	−0.957	+0.957
S_3	0	−0.707	+0.500	−0.500	+0.146	+0.146
α	0	+90.0°	−17.6°	+62.6°	−37.7°	+52.3°
ε	0	−22.5°	+15.0°	−15.0°	+4.2°	+4.2°
τ_o	0.853		0.978		0.978	

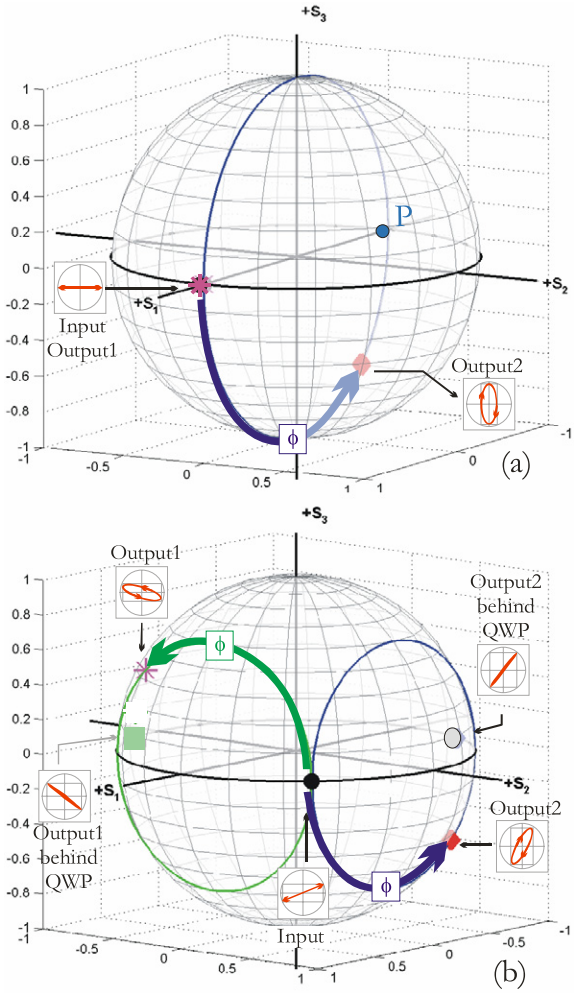

Figure 4. Poincaré sphere analysis for the FLC with phase shift mismatch ($\phi = 135°$, $\theta = \pi/4$). (a) Standard configuration with input polarizer oriented at 0°. (b) Optimized configuration with input polarizer oriented at 22.5°. Symbols (●), (∗) and (♦) denote, respectively, the input SOP and the output SOP1 and SOP2 behind the FLC modulator. Symbols (■) and (○) denote the final SOP1 and SOP2 in the optimized configuration after traversing the QWP oriented at −22.5°.

3.2. Contrast optimization

The Poincaré sphere analysis is now applied to find a polarization configuration that improves the contrast. The idea is based on the properties II and IV described in section 2. We look for the orientation of the input polarizer that yields two output SOPs with maximum orthogonality τ_o (i.e., two final points on the sphere with maximum antipodality). Then these two states can be further transformed by a QWP onto two quasi-linear orthogonal states, which can provide a high contrasted optical intensity signal.

This situation is obtained for an input linear SOP oriented at $\alpha_0 = 22.5°$, which corresponds to the point on the sphere bisecting the S_1 and S_2 axes. Figure 4(b) illustrates the corresponding transformations induced by the FLC modulator. The two sphere rotations around the S_1 and S_2 axes transform this input SOP onto two output states that lie on opposite sides of the sphere. Table 1 (central columns) shows the Stokes parameters and angles for these SOPs. These data and the geometry of figure 4(b) indicate that the two output SOPs share the same ellipticity but opposite helicity (they both have the same latitude, but in opposite hemispheres), and their azimuth has changed the same amount but in the opposite sense with respect to the input SOP. Therefore, the ellipticity and azimuth angles of the two SOPs emerging from the FLC modulator are related by

$$\varepsilon_2 = -\varepsilon_1. \tag{7a}$$

$$2\alpha_2 = \pi/2 - 2\alpha_1. \tag{7b}$$

These values can be related to the FLC phase shift ϕ by applying spherical trigonometric relations. The details are left for the appendix, and here we only give the results. The angles ε_1 and α_1 for the output SOP1 are given by

$$\sin(2\varepsilon_1) = \frac{\sin(\phi)}{\sqrt{2}}, \tag{8a}$$

$$\cos(2\alpha_1) = \frac{1}{\sqrt{1 + \cos^2(\phi)}}, \tag{8b}$$

where the sign of α_1 in equation (8*b*) is positive for ϕ in the ranges $[0, \pi/2]$ and $[3\pi/2, 2\pi]$, and it is negative if $\phi \in [\pi/2, 3\pi/2]$. In our particular case of $\phi = 135°$, we obtain $2\varepsilon_1 = 30°$ and $2\alpha_1 = -35.26°$. The corresponding values for the output SOP2 are given by equation (7), and are $2\varepsilon_2 = -30°$ and $2\alpha_2 = 125.26°$. The degree of orthogonality between these two states is $\tau_o = 0.978$, much higher than the value in the standard configuration.

However, these two emerging SOPs are far from the equator plane, and therefore they are not useful for high contrast intensity purposes. A QWP placed behind the FLC modulator can transform these states onto two states lying closer to the equator. One option could be orienting the QWP fast axis coincident with the azimuth of one of the states. This state will be transformed onto a linear state (property IV in section 2) and it can be fully extinguished with an analyzer oriented crossed to it. However, the other state will not be perfectly linear. A better option to optimize the contrast $c = |i_2 - i_1|$ is to orient the QWP at $-22.5°$. In this case none of the final states is perfectly linear, but the value of c is maximized by properly orienting the analyzer. The resulting final SOPs behind the QWP in such optimized configuration are also marked in figure 4(b), and their polarization parameters are also given in table 1 (right columns). These two final SOPs share the same ellipticity while their azimuth angles are complementary, i.e.:

$$\varepsilon'_2 = \varepsilon'_1, \tag{9a}$$

$$2\alpha'_2 = \pi + 2\alpha'_1, \tag{9b}$$

where the prime symbol denotes the angles for the final SOPs behind the QWP. The angles $(\varepsilon'_1, \alpha'_1)$ of the final SOP1 can be related to the corresponding angles behind the FLC $(\varepsilon_1, \alpha_1)$ by means of spherical trigonometric relations. Once again, the details are given in the appendix and here we give the results:

$$\sin(2\varepsilon'_1) = \cos(2\varepsilon_1)\sin\left(\frac{\pi}{4} + 2\alpha_1\right). \tag{10a}$$

$$\cos\left(2\alpha'_1 + \frac{\pi}{4}\right) = \frac{\cos(2\varepsilon_1)\cos(\frac{\pi}{4} + 2\alpha_1)}{\sqrt{1 - \cos^2(2\varepsilon_1)\sin^2(\frac{\pi}{4} + 2\alpha_1)}}. \tag{10b}$$

Taking into account equations (8), these values can be related to the phase shift (ϕ) introduced by the FLC modulator, and the following expressions can be derived:

$$\sin(2\varepsilon'_1) = \cos^2\left(\frac{\phi}{2}\right). \tag{11a}$$

$$\cos\left(2\alpha'_1 + \frac{\pi}{4}\right) = \frac{1 - \cos\phi}{\sqrt{4 - (1 + \cos\phi)^2}}. \tag{11b}$$

In the case where $\phi = 135°$, equations (11) and (9) lead to the ellipticity $\varepsilon'_1 = 4.2°$ and the azimuth $2\alpha'_1 = -75.36°$ for the final SOP1, while they are $\varepsilon'_2 = 4.2°$ and $2\alpha'_2 = 104.64°$ for the final SOP2. As expected, the orthogonality between the two SOPs is maintained at $\tau_o = 0.978$ after traversing the QWP. Let us note that their azimuths are perpendicular and their ellipticity is very small. Therefore, they are useful states to yield a highly contrasted intensity signal, which is achieved by orienting the analyzer with the same azimuth as one of these output states. For instance, we oriented the analyzer parallel to the azimuth of the second state ($\theta_P = 52.3°$).

The intensity transmitted by the analyzer is derived by applying the generalized Malus law (property V in section 2). The angles between the SOP fully transmitted by the analyzer and the two final output SOPs are directly given by their ellipticities as $\gamma_1 = 2\varepsilon'_1$ and $\gamma_2 = \pi - 2\varepsilon'_1$, respectively. Therefore the corresponding intensities are

$$i_1 = \cos^2\left(\frac{\gamma_1}{2}\right) = \cos^2(\varepsilon'_1), \tag{12a}$$

$$i_2 = \cos^2\left(\frac{\gamma_2}{2}\right) = \cos^2\left(\frac{\pi}{2} - \varepsilon'_1\right) = \sin^2(\varepsilon'_1). \tag{12b}$$

These final intensities can be related to the phase shift (ϕ) introduced by the FLC modulator by means of equation (11*a*), and the result is

$$i_1 = \frac{1}{2}\left(1 + \sqrt{1 - \cos^4\left(\frac{\phi}{2}\right)}\right), \tag{13a}$$

$$i_2 = \frac{1}{2}\left(1 - \sqrt{1 - \cos^4\left(\frac{\phi}{2}\right)}\right). \tag{13b}$$

Therefore, the contrast in this case is given by the relation

$$c = |i_2 - i_1| = \sqrt{1 - \cos^4\left(\frac{\phi}{2}\right)}. \tag{14}$$

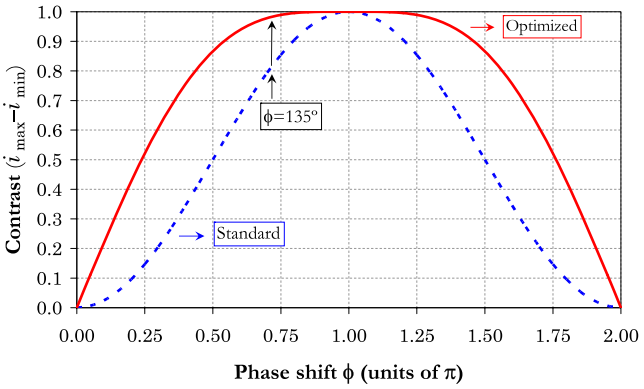

Figure 5. Theoretical contrast ($c = |i_2 - i_1|$) as a function of the phase shift (ϕ) introduced by the FLC modulator in the standard (equation (6)) and optimized (equation (14)) configurations. The expected contrast values for the case where $\phi = 135°$ are indicated.

This optimized contrast function is represented in figure 5 together with that for the standard configuration (equation (6)). It shows that the optimized configuration gives a better contrast than the standard configuration for all values of ϕ. For our case where $\phi = 135°$, we obtain a contrast value for the optimized configuration of $c = 0.989$.

3.3. Contrast optimization with the QWP placed in front of the modulator

Because of the symmetry properties of reciprocal polarization devices [25], the contrast results in the optimized configuration analyzed in figure 4(b), in which the QWP was placed behind the FLC modulator, can be also reproduced with a configuration in which the QWP is placed in front of the FLC modulator. This configuration can be used to generate an input elliptical SOP that yields two SOPs emerging from the FLC modulator which are as close as possible to being

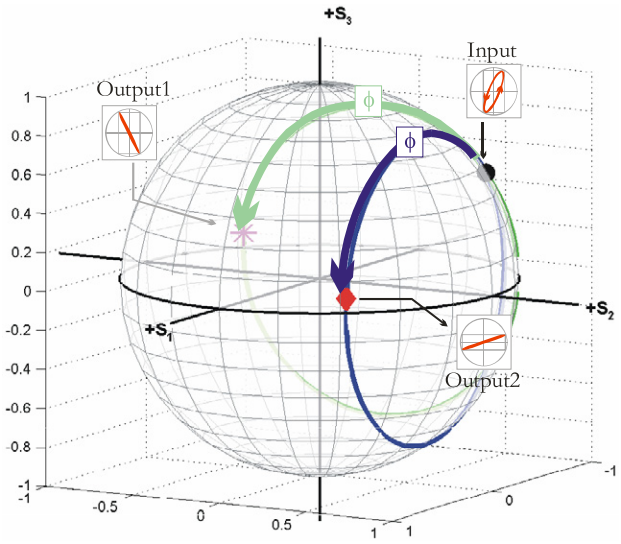

Figure 6. Poincaré sphere analysis for the optimized configuration proposed in [15], with input polarizer oriented at 52.3°, and a QWP in front of the FLC modulator oriented at −22.5°. Symbols (●), (∗) and (♦) denote the input, output1, and output2 SOPs.

linear and orthogonal. Results with this configuration were already presented in our previous work [15], where we merely performed a numerical search of the orientations of the polarization components leading to the best contrast. The present Poincaré analysis provides the physical insights into those results. The optimized configuration presented in [15] had the input polarizer oriented at 52.3°, and the QWP (in front of the FLC modulator) at −22.5°, and the analyzer was oriented at 22.5°. Let us note that this configuration is obtained by reversing the elements in the configuration described in section 3.2, thus providing equivalent results. Figure 6 shows the input and output SOPs generated with this system, and table 2 summarizes the corresponding polarization parameters. Following similar considerations as in the previous subsection, it can be shown that equation (14) is also valid for the optimized configuration with the QWP placed in front of the modulator. The theoretical curves presented in figure 5 are in perfect agreement with the equivalent ones obtained numerically in [15], thus being a relevant result in this new paper.

Finally, we explored the use of two QWPs, one in front and the other behind the FLC modulator, in order to further improve the contrast. The results showed that the contrast cannot be enhanced because the intensity values remain constant.

4. Experimental verification

The above analysis was verified experimentally by means of a commercial FLC modulator from CRL-Opto, model LCS2N-G. This is a single-pixel FLC modulator, with a squared active area of 25.5 × 25.5 mm^2, designed to operate at the green wavelength $\lambda = 540$ nm. We show how its performance as intensity modulator is degraded by the use of a different wavelength (in our case $\lambda = 633$ nm from a He–Ne laser), and how this effect can be compensated following the previously described approach.

Table 2. Polarization parameter values for the optimized configuration proposed in [15] in which the input illumination is elliptically polarized (figure 6).

	Optimized configuration with input elliptical SOP (figure 6)		
	Input	Output1	Output2
S_1	−0.610	−0.610	+0.789
S_2	+0.610	−0.789	+0.610
S_3	+0.506	+0.073	+0.073
α	+67.5°	−63.8°	+18.8°
ε	+15.2	+2.1°	+2.1°
τ_o		0.978	

We have previously calibrated the modulator's physical parameters [15], including the location of the neutral axes, its rotation with the applied voltage (which was verified to be $\Delta\theta = \pi/4$), and the phase shift dispersion. For our illuminating wavelength $\lambda = 633$ nm, the wavelength deviation with respect to the ideal value of 540 nm results in a phase shift decrease from the ideal half-wave-plate performance. We experimentally measured a value $\phi = 135°$. Figure 7 shows the detected optical signal when a bipolar 10 V_{pp}, DC balanced, square voltage of frequency 100 Hz is addressed to the modulator. The modulated beam is measured with a Thorlabs detector (PDA55 model) whose output signal is displayed on an oscilloscope. For every detected optical signal, we also measured the complementary signal obtained by rotating 90° the final analyzer. The data are normalized by dividing each value by the sum of itself and its corresponding complementary value. Results in figure 7 show the normalized signals corresponding to the three cases analyzed in the previous section.

Figure 7(a) corresponds to the standard configuration analyzed in figure 4(a), with the FLC placed between two crossed polarizers. We can observe that the optical signal switches every 5 ms, between a dark and a bright state. However, the bright state does not reach 100% transmission because of the phase shift mismatch. Figures 7(b) and (c) show the results for the two optimized configurations described in figures 4(b) and 6, respectively. In figure 7(b), linearly polarized light oriented at 22.5° illuminates the FLC, and the two emerging SOPs are transformed onto quasi-linear states by a QWP placed behind the modulator and oriented at −22.5°. The analyzer is here oriented at 52.3°. In figure 7(c) the QWP is placed before the modulator to generate an input elliptical SOP that after traversing the FLC modulator yields two quasi-linear and orthogonal states. This is the reversed configuration compared to the previous one, i.e. the input polarizer is oriented at 52.3°, the QWP is at −22.5°, and the analyzer is oriented at 22.5°. The result in both cases is a high contrasted optical signal, now reaching almost perfect 100% intensity transmission.

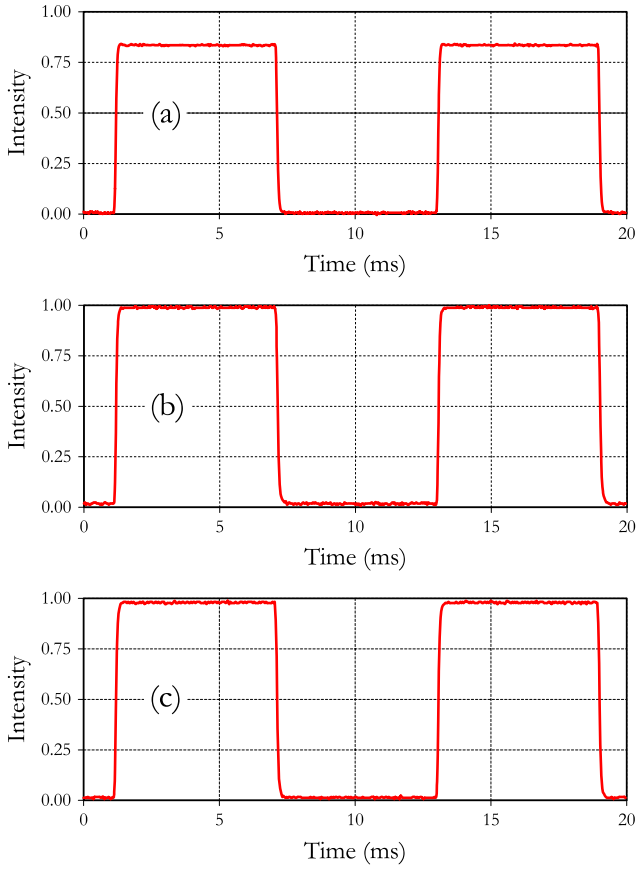

Figure 7. Experimental intensity signal detected when the FLC modulator is illuminated with $\lambda = 633$ nm (phase shift $\phi = 135°$) and is addressed with a bipolar 100 Hz electrical voltage (10 V_{pp}, DC balanced). (a) Standard configuration analyzed in figure 4(a). (b)–(c) Optimized configurations with elliptical polarizations described in figures 4(b) and 6 respectively.

5. Conclusions

In summary, we have analyzed the optical performance of an FLC modulator as a switching device for binary intensity modulation using the Poincaré formalism. Within this framework, we provide a description of the device performance as a function of the phase shift, and an analytical demonstration and physical interpretation of a previously reported numerical technique to optimize the contrast when the phase shift differs from the ideal value $\phi = \pi$. The optimization of the optical contrast is reduced to a geometrical problem. Using spherical trigonometric relations we provide analytical expressions for the intensity contrast as a function of the phase shift ϕ for both the standard and the optimized configurations. Finally, the proposed ideas have been verified with a commercial single-pixel FLC modulator, using a He–Ne laser with wavelength 633 nm, for which the phase shift is 135°. This technique may be useful in enlarging the number of wavelengths for which the FLC modulator is a useful device, or in applying its modulation properties to polychromatic sources.

Acknowledgments

This work was supported by Fondo Europeo de Desarrollo Regional (FEDER) funds and the Ministerio de Educación y Cultura from Spain (projects FIS2006-13037-C02-02 and FIS2007-60626).

Appendix

In this appendix we demonstrate the relations for the ellipticity and azimuth angles for the final SOP1 as a function of the phase shift (ϕ) in the optimized configuration shown in figure 4(b). This can be done by applying trigonometric relations to the spherical triangles defined on the surface of the Poincaré sphere.

We start by deriving the ellipticity (ε_1) and azimuth (α_1) of the output SOP1 behind the FLC modulator. In this case, the input linear SOP is oriented at 22.5° (black dot in figure 4(b)), and is transformed onto output SOP1 (purple marker in figure 4(b)) upon a rotation by angle ϕ around the S_1 axis. Figure A.1 shows the same transformation as figure 4(b) (i.e., they correspond to the specific value $\phi = 135°$), but with a different point of view in order to clearly visualize the spherical triangles used in the demonstration. We consider the triangle ABC. Point A is on the S_1 axis, and point B is the output SOP1. The angular sectors of this spherical triangle are AB $= \pi/4$, CB $= 2\varepsilon_1$, and AC $= 2\alpha_1$, as indicated in the figure. The angles at points A and C are $\pi - \phi$ and $\pi/2$, respectively. Therefore, applying the sine and cosine laws directly leads to the two following relations:

$$\sin\left(\frac{\pi}{4}\right) = \frac{\sin(2\varepsilon_1)}{\sin(\pi - \phi)}, \tag{A.1}$$

$$\cos\left(\frac{\pi}{4}\right) = \cos(2\varepsilon_1)\cos(2\alpha_1). \tag{A.2}$$

The derivations of equation (8) in the text are straightforward from these two equations.

Next, this output state is transformed by a QWP oriented with its fast axis at −22.5°. This means that point B is transformed onto point E (green square in figure A.1) through a $\pi/2$-rotation around the axis defined by point F. The ellipticity (ε_1') and azimuth (α_1') of the final SOP behind the QWP are given, respectively, by segments DE $= 2\varepsilon_1'$ and AD $= -\alpha_1'$ (let us note that α_1' is negative in this case). These angles ($\varepsilon_1', \alpha_1'$) can be related to the corresponding values (ε_1, α_1) for the SOP before the QWP by analyzing trigonometric relations on the spherical triangles CBF and FED in figure A.1. First, let us note that the segments FB and FE are equal, and we denote them by x. Note also that the distance FC is $\pi/4 + 2\alpha_1$, where the negative sign of α_1 in figure A.1 has been considered (the same relation holds if α_1 is positive). The application of the cosine and sine rules to the spherical triangle CBF yields the following relations:

$$\cos x = \cos(2\varepsilon_1)\cos\left(\frac{\pi}{4} + 2\alpha_1\right), \tag{A.3}$$

$$\cos(2\varepsilon_1) = \cos\left(\frac{\pi}{4} + 2\alpha_1\right)\cos x + \sin\left(\frac{\pi}{4} + 2\alpha_1\right)\sin x \cos\beta, \tag{A.4}$$

$$\sin x = \frac{\sin(2\varepsilon_1)}{\sin\beta}, \tag{A.5}$$

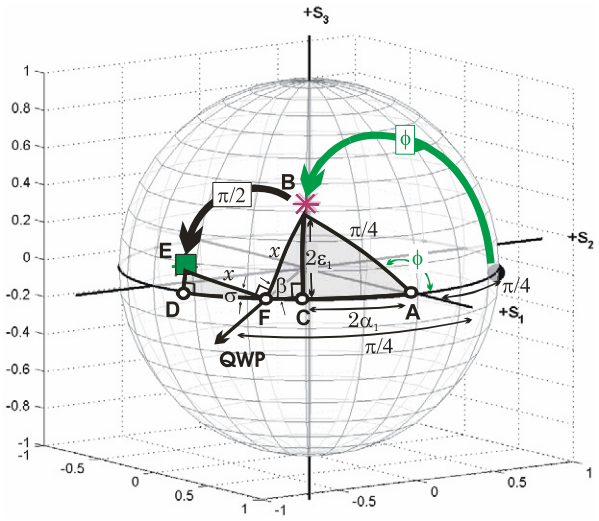

Figure A.1. Poincaré sphere transformations in figure 4(b) presented with a different view for a better visualization of the spherical triangles used in the derivations. Symbols (●), (∗) and (■) denote the input SOP, the output SOP1 behind the FLC modulator, and the output SOP1 behind the QWP.

where β is the angle at point F. On the other hand, the application of the cosine and sine laws to the spherical triangle FED leads to the following relations:

$$\cos x = \cos(2\varepsilon_1') \cos\left(2\alpha_1' + \frac{\pi}{4}\right), \tag{A.6}$$

$$\sin x = \frac{\sin(2\varepsilon_1')}{\sin\sigma}, \tag{A.7}$$

where σ is the angle inside triangle FED at point F. Figure A.1 shows that the angles β and σ are related as $\sigma = \pi/2 - \beta$, which can be applied to equation (A.7) to become

$$\sin x = \frac{\sin(2\varepsilon_1')}{\cos\beta}. \tag{A.8}$$

Combination of equations (A.8) and (A.4) directly leads to the relation

$$\sin(2\varepsilon_1') = \cos(2\varepsilon_1) \sin\left(\frac{\pi}{4} + 2\alpha_1\right), \tag{A.9}$$

which coincides with equation (10*a*) in the text. Similarly, from equations (A.3) and (A.6) we obtain

$$\cos\left(2\alpha_1' + \frac{\pi}{4}\right) = \frac{\cos(2\varepsilon_1)\cos\left(\frac{\pi}{4} + 2\alpha_1\right)}{\sqrt{1 - \sin^2(2\varepsilon_1')}}, \tag{A.10}$$

which yields equation (10*b*) in the text when combined with equation (A.9).

References

[1] Bougrenet de la Tocnaye J L and Dupont L 1997 Complex amplitude modulation by use of a liquid crystal spatial light modulators *Appl. Opt.* **36** 1730–41

[2] Osten W, Kohler C and Liesener J 2005 Evaluation application of spatial light modulators for optical metrology *Opt. Pura Apl.* **38** 71–81

[3] Yeh P and Gu C 1999 *Optics of Liquid Crystal Displays* (New York: Wiley)

[4] Giallorenzi T G, Weiss J A and Sheridan J P 1976 Light scattering from smectic liquid crystal waveguide *J. Appl. Phys.* **47** 1820–6

[5] Moddel G 1995 Ferroelectric liquid crystal spatial light modulators *Spatial Light Modulator Technology* ed U Efron (New York: Dekker) chapter 6, pp 287–359

[6] Underwood I 1997 Ferroelectric liquid crystal over silicon spatial light modulators—principles practice prospects *Spatial Light Modulators* (*OSA Trends in Optics and Photonics* vol 14) ed G Burdge and S C Esener (Washington, DC: Optical Society of America) pp 76–88

[7] Gros E and Dupont L 2001 Ferroelectric liquid crystal optical waveguide switches using the double-refraction effect *IEEE Photon. Technol. Lett.* **13** 115–7

[8] Sirleto L, Coppola G, Breglio G, Abbate G, Righini G C and Otón J M 2002 Electro-optical switch continuously tunable filter based on a Bragg grating in a planar waveguide with a liquid crystal overlayer *Opt. Eng.* **41** 2890–8

[9] Hariharan P and Ciddor P E 1997 Achromatic switchable polarization rotators *Opt. Eng.* **36** 952–6

[10] Hariharan P and Ciddor P E 1999 Improved switchable achromatic phase shifters *Opt. Eng.* **38** 1078–80

[11] Manolis I G, Wilkinson T D, Redmond M M and Crossland W A 2002 Reconfigurable multilevel phase holograms for optical switches *IEEE Photon. Technol. Lett.* **14** 801–3

[12] Hossak W J, Theofanidou E, Crain J, Heggarty K and Birch M 2003 High-speed holographic optical tweezers using a ferroelectric liquid crystal microdisplay *Opt. Express* **11** 2053–9

[13] Gießelmann F, Langhoff A and Zugenmaier P 1997 Dispersion of the optical axes in smectic C* liquid crystals *Liq. Cryst.* **23** 927–31

[14] Surguy P 1998 How ferroelectric liquid-crystal devices works *Inf. Disp.* **2** 24–7

[15] Martínez A, Beaudoin N, Moreno I, Sánchez-López M M and Velásquez P 2006 Optimization of the contrast ratio of a ferroelectric liquid crystal optical modulator *J. Opt. A: Pure Appl. Opt.* **8** 1013–8

[16] Davis J A, Moreno I and Tsai P 1998 Polarization eigenstates for twisted-nematic liquid crystals displays *Appl. Opt.* **37** 937–45

[17] Nicolás J, Campos J and Yzuel M J 2002 Phase amplitude modulation of elliptic polarization states by nonabsorbing anisotropic elements: application to liquid-crystal devices *J. Opt. Soc. Am.* A **19** 1013–20

[18] Bigelow J E and Kashnow R A 1977 Poincaré sphere analysis of liquid crystal optics *Appl. Opt.* **16** 2090–6

[19] Johnson M 1981 Poincaré sphere representation of birefringent networks *Appl. Opt.* **20** 2075–2080

[20] Zhuang Z, Kim Y J and Patel J S 1999 Parameter optimization for a reflective bistable twisted nematic display by use of the Poincaré sphere method *Opt. Lett.* **24** 1166–8

[21] Durán V, Lancis J, Tajahuerce E and Climent V 2007 Poincaré sphere method for optimizing the phase modulation response of a twisted nematic liquid crystal display *J. Disp. Technol.* **3** 41883

[22] Zhang Y, Wang B, Chung D B and Bos P J 2004 Poincaré sphere analysis of reflective liquid crystal device *Japan. J. Appl. Phys.* **43** 7125–8

[23] Huard S 1997 *Polarization of Light* (New York: Wiley)

[24] Dettwiller L 2001 Interpretation generalization of polarized light interferences by means of the Poincaré sphere *Eur. J. Phys.* **22** 575–86

[25] Fernández-Pousa C R, Moreno I, Bennis N and Gómez-Reino C 2000 Generalized formulation and symmetry properties of reciprocal nonabsorbing polarization devices: application to liquid-crystal displays *J. Opt. Soc. Am.* A **17** 2074–80